

Asymmetric crystallization during cooling and heating in model glass-forming systemsMinglei Wang,^{1,2} Kai Zhang,^{1,2} Zhusong Li,³ Yanhui Liu,^{1,2} Jan Schroers,^{1,2} Mark D. Shattuck,^{1,3} and Corey S. O'Hern^{1,2,4,5}¹*Department of Mechanical Engineering and Materials Science, Yale University, New Haven, Connecticut 06520, USA*²*Center for Research on Interface Structures and Phenomena, Yale University, New Haven, Connecticut 06520, USA*³*Department of Physics and Benjamin Levich Institute, The City College of the City University of New York, New York, New York 10031, USA*⁴*Department of Physics, Yale University, New Haven, Connecticut 06520, USA*⁵*Department of Applied Physics, Yale University, New Haven, Connecticut 06520, USA*

(Received 8 January 2015; published 17 March 2015)

We perform molecular dynamics (MD) simulations of the crystallization process in binary Lennard-Jones systems during heating and cooling to investigate atomic-scale crystallization kinetics in glass-forming materials. For the cooling protocol, we prepared equilibrated liquids above the liquidus temperature T_l and cooled each sample to zero temperature at rate R_c . For the heating protocol, we first cooled equilibrated liquids to zero temperature at rate R_p and then heated the samples to temperature $T > T_l$ at rate R_h . We measured the critical heating and cooling rates R_h^* and R_c^* , below which the systems begin to form a substantial fraction of crystalline clusters during the heating and cooling protocols. We show that $R_h^* > R_c^*$ and that the asymmetry ratio R_h^*/R_c^* includes an intrinsic contribution that increases with the glass-forming ability (GFA) of the system and a preparation-rate dependent contribution that increases strongly as $R_p \rightarrow R_c^*$ from above. We also show that the predictions from classical nucleation theory (CNT) can qualitatively describe the dependence of the asymmetry ratio on the GFA and preparation rate R_p from the MD simulations and results for the asymmetry ratio measured in Zr- and Au-based bulk metallic glasses (BMG). This work emphasizes the need for and benefits of an improved understanding of crystallization processes in BMGs and other glass-forming systems.

DOI: [10.1103/PhysRevE.91.032309](https://doi.org/10.1103/PhysRevE.91.032309)

PACS number(s): 64.70.pe, 64.70.Q-, 61.43.Fs, 61.66.Dk

I. INTRODUCTION

Crystallization, during which a material transforms from a dense, amorphous liquid to a crystalline solid, occurs via the nucleation and subsequent growth of small crystalline domains [1]. Crystallization in metals has been intensely studied over the past several decades with the goal of developing the ability to tune the microstructure to optimize the mechanical properties of metal alloys [2–4]. However, *in situ* observation of crystallization in metallic melts is limited due to the rapid crystallization kinetics of metals [5–7].

In contrast, bulk metallic glasses (BMGs), which are amorphous metal alloys, can be supercooled to temperatures below the solidus temperature T_s and persist in a dense, amorphous liquid state over more than 12 orders of magnitude in time scales or viscosity [8]. Deep supercooling of BMGs provides the ability to study crystallization on time scales that are accessible to experiments [9–12].

These prior experimental studies have uncovered fundamental questions concerning crystallization kinetics in BMGs. For example, when a BMG in the glass state is heated to a temperature $T_f < T_s$ in the supercooled liquid region, crystallization is much faster than crystallization that occurs when the metastable melt is cooled to the same temperature T_f [13,14]. Asymmetries in the crystallization time scales upon heating versus cooling of up to two orders of magnitude have been reported in experiments [15,16]. The asymmetry impacts industrial applications of BMGs because rapid crystallization upon heating limits the thermoplastic forming processing time window for BMGs [17–20].

Recent studies have suggested that the asymmetry in the crystallization time scales originates from the temperature dependence of the nucleation and growth rates [15], i.e., that the nucleation rate is maximal at a temperature below

that at which the growth rate is maximal. According to this argument, crystallization upon heating is faster because of the growth of the nascent crystal nuclei that formed during the thermal quench to the glass. In contrast, crystallization is slower upon cooling since crystal nuclei are not able to form at high temperatures in the melt. However, there has been no direct visualization of the crystallization process in BMGs, and it is not yet understood why the asymmetry varies from one BMG to another [21] and how sensitively the asymmetry depends on the cooling rate R_p used to prepare the glass. An improved, predictive understanding of the crystallization process in BMGs will aid the design of new BMG-forming alloys with small crystallization asymmetry ratios and large thermoplastic processing time windows.

We employ molecular dynamics (MD) simulations of bidisperse spheres interacting via Lennard-Jones potentials [22–24] to visualize directly the crystallization process upon heating and cooling in model metallic glass-forming systems. We perform thermal quenches of the system from a high-temperature T_i in the equilibrated liquid regime to a glass at $T_f = 0$ and vary the cooling rate R_c by several orders of magnitude. For cooling rates below the critical cooling rate $R_c < R_c^*$, the system begins to crystallize, whereas for $R_c > R_c^*$, the system remains amorphous. We also performed MD simulations in which we heat the zero-temperature glassy states (prepared at cooling rate $R_p > R_c^*$) through the supercooled liquid regime to $T_f = T_l$ over a range of heating rates R_h . For heating rates $R_h < R_h^*$, the system begins to crystallize, whereas for $R_h > R_h^*$, it remains amorphous. We also find that the critical heating rate has an intrinsic contribution $R_h^*(\infty)$ and an R_p -dependent contribution $R_h^*(R_p) - R_h^*(\infty)$ that increases with decreasing R_p . We measured the asymmetry ratio R_h^*/R_c^* as a function of the glass-forming ability (GFA) and R_p for several binary Lennard-Jones mixtures and find that $R_h^*/R_c^* > 1$ and the ratio

grows with increasing GFA and decreasing R_p . We show that these results are consistent with predictions from classical nucleation theory (CNT) that the maximal growth rate occurs at a higher temperature than the maximal nucleation rate and that the separation between the nucleation and growth peaks increases with the GFA. Further, CNT is able to qualitatively recapitulate the dependence of the asymmetry ratio on the GFA as measured through R_c^* for both our MD simulations and recent experiments on BMGs as well as on R_p for the MD simulations [25].

The remainder of the manuscript is organized into three sections: In Sec. II, we describe the MD simulations of binary Lennard-Jones mixtures, the computational methods to detect and structurally characterize crystal nuclei, and measurements of the critical cooling and heating rates, R_c^* and R_h^* . In Sec. III, we show results from MD simulations for the time-temperature transformation diagram [26] and the asymmetry ratio R_h^*/R_c^* as a function of the glass-forming ability as measured by the critical cooling rate R_c^* and the cooling rate used to prepare the zero-temperature glasses R_p . We also compare our simulation results for the asymmetry ratio to experimental measurements of the ratio for two BMGs and to predictions of the ratio from classical nucleation theory. In Sec. IV, we briefly summarize our results and put forward our conclusions.

II. METHODS

We performed MD simulations of binary Lennard-Jones (LJ) mixtures of $N = N_A + N_B$ spheres with mass m at constant volume $V = L^3$ in a cubic simulation box with side length L and periodic boundary conditions. We studied mixtures with $N_A = N_B$ and diameter ratio $\alpha = \sigma_B/\sigma_A < 1$. We employed the LJ pairwise interaction potential between spheres i and j :

$$u(r_{ij}) = 4\epsilon[(\sigma_{ij}/r_{ij})^{12} - (\sigma_{ij}/r_{ij})^6], \quad (1)$$

where r_{ij} is their center-to-center separation, ϵ is the depth of the minimum in the potential energy $u(r_{ij})$, $\sigma_{ij} = (\sigma_i + \sigma_j)/2$, and $u(r_{ij})$ has been truncated and shifted so that the potential energy and force vanish for separations $r_{ij} \geq 3.5\sigma_{ij}$ [27]. We varied the system volume V to fix the packing fraction $\phi = \pi\sigma_A^3(N_A + \alpha^3 N_B)/6V = 0.5236$ [28] at each diameter ratio α . For most simulations, we considered $N = 1372$ spheres, but we also studied $N = 4000$ and 8788 to assess finite-size effects. Below, energy, length, time, and temperature scales are expressed in units of ϵ , σ_A , $\sigma_A\sqrt{m/\epsilon}$, and ϵ/k_B , respectively, where the Boltzmann constant k_B has been set to be unity.

A. Cooling and heating protocols

For each particle diameter ratio, which yield different glass-forming abilities, we performed MD simulations to cool metastable liquids to zero temperature and heat zero-temperature glasses into the metastable liquid regime to measure R_c^* and R_h^* at which the systems begin to crystallize. To measure R_c^* , we first equilibrate the system at high temperature $T_i = 2.0$ using a Gaussian constraint thermostat [27]. We then cool the system by decreasing the temperature linearly at rate R_c from T_i to $T_f = 0$:

$$T(t) = T_i - R_c t. \quad (2)$$

To measure the critical heating rate $R_h^*(R_p)$ at finite rate R_p , we first prepare the systems in a glass state by cooling them from the high-temperature liquid state to zero temperature at rate $R_p > R_c^*$. To measure the intrinsic critical heating rate $R_h^*(\infty)$, we quench the systems infinitely fast to zero temperature using conjugate gradient energy minimization. For both cases, we heat the zero-temperature glasses using a linear ramp,

$$T(t) = R_h t, \quad (3)$$

until $T_f = 2.0$. For both heating and cooling protocols, we carried out $N_{\text{tot}} = 1000$ independent trajectories and averaged the results.

B. Identification of crystal nuclei

To detect the onset of crystallization in our simulations [15], we differentiate “crystal-like” versus “liquid-like” particles based on the value of the area-weighted bond orientational order parameter for each particle [29–31]. We define the complex-valued bond orientational order parameter for particle i :

$$q_{lm}(i) = \frac{\sum_{j=1}^{N_b} A_{ij} Y_{lm}[\theta(\vec{r}_{ij}), \phi(\vec{r}_{ij})]}{\sum_{j=1}^{N_b} A_{ij}}, \quad (4)$$

where $Y_{lm}[\theta(\vec{r}_{ij}), \phi(\vec{r}_{ij})]$ is the spherical harmonic of degree l and order m , $\theta(\vec{r}_{ij})$ and $\phi(\vec{r}_{ij})$ are the polar and azimuthal angles for the vector \vec{r}_{ij} , $j = 1, \dots, N_b$ gives the index of the Voronoi neighbors of particle i , and A_{ij} is the area of the face of the Voronoi polyhedron common to particles i and j . The correlation coefficient [29] between the bond orientational order parameters $q_{lm}(i)$ and $q_{lm}(j)$, where particle j is a Voronoi neighbor of i , and

$$S_{ij} = \frac{\sum_{m=-6}^6 q_{6m}(i) q_{6m}^*(j)}{[\sum_{m=-6}^6 |q_{6m}(i)|^2]^{1/2} [\sum_{m=-6}^6 |q_{6m}(j)|^2]^{1/2}} \quad (5)$$

is sensitive to face-centered-cubic (FCC) order. When $S_{ij} > 0.7$, i and j are considered “connected.” If particle i has more than 10 connected Voronoi neighbors, it is defined as “crystal-like.” The ratio N_{cr}/N gives the fraction of crystal-like particles in a given configuration. In addition, we also define a crystal cluster as the set of crystal-like particles that possess mutual Voronoi neighbors. Distinct crystal clusters that nucleate and grow upon heating and cooling are shown in Fig. 1.

This general scheme for identifying crystal-like particle clusters has been implemented in prior studies [33–35]; however, we made two improvements [36]. First, we defined nearest-neighbor particles by Voronoi tessellation to remove the arbitrariness associated with defining neighbors using a cutoff distance. Second, the definition of the bond orientational order parameter q_{lm} weights each bond between the central particle and its nearest neighbors by the area of the associated Voronoi polyhedral face, such that q_{lm} is a continuous function of particle coordinates.

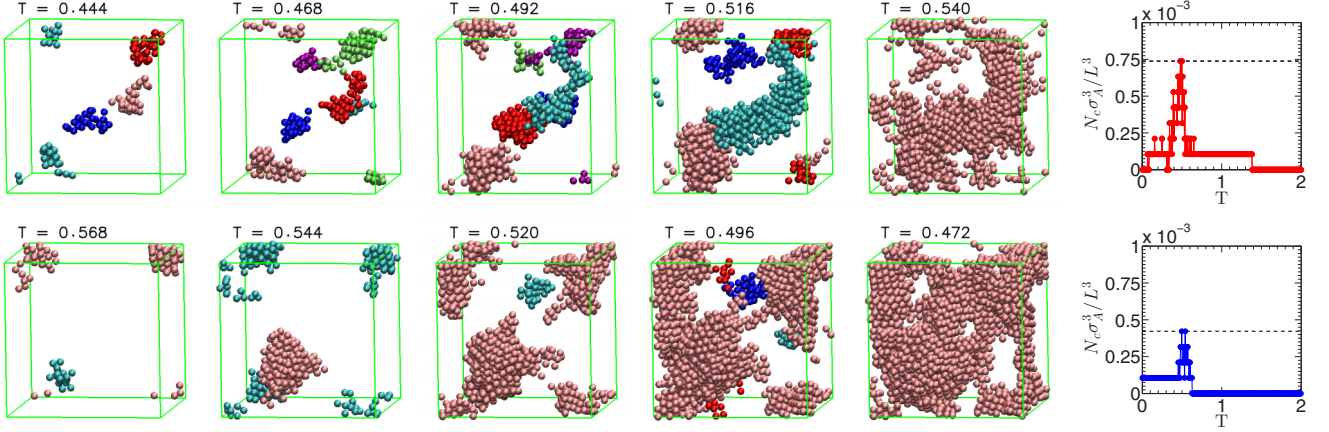


FIG. 1. (Color online) Snapshots of the nucleation and growth of crystal clusters at several temperatures T as a monodisperse Lennard-Jones system is heated from zero temperature to $T_f = 2.0$ at a rate $R_h < R_h^*$ (top row) and cooled from initial temperature $T_i = 2.0$ to zero temperature at a rate $R_c < R_c^*$ (bottom row). Distinct, disconnected crystal nuclei are identified using the technique in Ref. [32] and are shaded different colors. The far-right panel indicates the number of clusters N_c normalized by L^3/σ_A^3 as a function of temperature during a typical heating (top) and cooling (bottom) trajectory. The maximum number of clusters N_c^{\max} is indicated by the horizontal dashed line.

C. Probability for crystallization

For each diameter ratio and rate, we measure the probability for crystallization $P(R_{h,c}) = N_X/N_{\text{tot}}$, where N_X is the number of trajectories that crystallized with $N_{\text{cr}}/N > 0.5$ during the heating or cooling protocol and N_{tot} is the total number of trajectories (cf. insets to Fig. 2). We find that the data for $P(R_{h,c})$ collapses onto a sigmoidal scaling function as shown

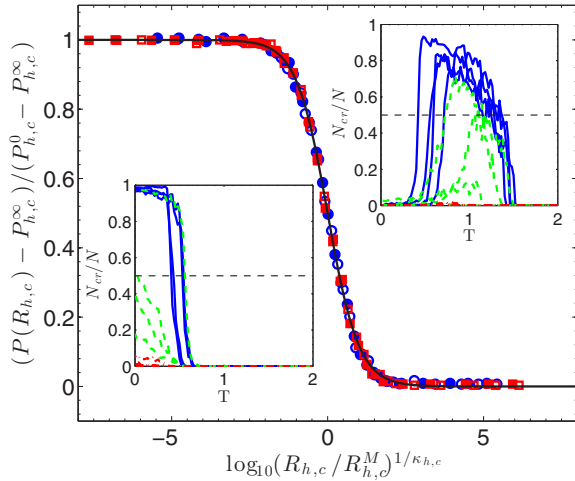


FIG. 2. (Color online) Shifted and normalized probability for crystallization $[P(R_{h,c}) - P_{h,c}^\infty]/(P_{h,c}^0 - P_{h,c}^\infty)$ versus the scaled heating or cooling rate $\log_{10}(R_{h,c}/R_{h,c}^M)^{1/\kappa_{h,c}}$. Circles (squares) indicate data for cooling (heating) for diameter ratios $\alpha = 1.0$ (filled symbols) and 0.97 (open symbols). The insets show the fraction of crystal-like particles N_{cr}/N as a function of temperature T during cooling (lower left) and heating (upper right) for 12 configurations with $\alpha = 1.0$. The four solid, dashed, and dot-dashed curves in each inset correspond to cooling and heating trajectories with rates slower than $R_{h,c}^*$, near $R_{h,c}^*$, and faster than $R_{h,c}^*$, respectively. Trajectories for which N_{cr}/N exceeds 0.5 (above the horizontal dashed line) are considered to have crystallized during the heating or cooling protocol.

in Fig. 2:

$$\frac{(P(R_{h,c}) - P_{h,c}^\infty)}{P_{h,c}^0 - P_{h,c}^\infty} = \frac{1}{2} \left\{ 1 - \tanh \left[\log_{10} \left(\frac{R_{h,c}}{R_{h,c}^M} \right)^{1/\kappa_{h,c}} \right] \right\}, \quad (6)$$

where $P_{h,c}^\infty$ is the probability for crystallization in the limit of infinitely fast rates $R_{h,c} \rightarrow \infty$, $P_{h,c}^0$ is the probability for crystallization in the $R_{h,c} \rightarrow 0$ limit, $R_{h,c}^M$ is the rate at which $P(R_{h,c}) = (P_{h,c}^0 + P_{h,c}^\infty)/2$, and $\kappa_{h,c}$ is the stretching factor. We find that $\kappa_c \approx 0.25$ and $\kappa_h \approx 0.2$ for $\alpha = 1.0$, and these factors increase by only a few percent over the range in α that we consider. We define the critical heating and cooling rates R_h^* and R_c^* by the rates at which $P(R_{h,c}) = 0.5$, i.e.,

$$R_{h,c}^* = R_{h,c}^M 10^{\kappa_{h,c} \tanh^{-1} \left[\frac{P_{h,c}^0 + P_{h,c}^\infty - 1}{P_{h,c}^0 - P_{h,c}^\infty} \right]}. \quad (7)$$

As shown in the insets to Fig. 2, for $R_{h,c} \ll R_{h,c}^*$ most of the configurations crystallize during heating or cooling. In contrast, for $R_{h,c} \gg R_{h,c}^*$, none of the configurations crystallize.

III. RESULTS

An advantage of MD simulations is that they can provide atomic-level structural details of the crystallization dynamics that are often difficult to obtain in experiments. In Fig. 1, we visualize the nucleation and growth of clusters of crystal-like particles during the heating and cooling simulations. In both cases, the number of clusters reaches a maximum near $T \approx 0.5$. In Fig. 3, we show the maximum number of clusters N_c^{\max} (normalized by L^3/σ_A^3) that form during the heating and cooling protocols. We find that more crystal clusters form during the heating protocol compared to the cooling protocol for all particle diameter ratios studied, which is supported by the measured time-temperature-transformation (TTT) diagram. In addition, we will show below that the

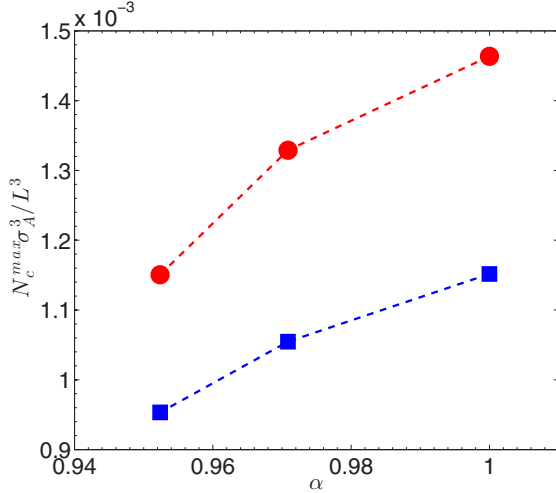


FIG. 3. (Color online) Maximum value N_c^{\max} of the number of crystal clusters $N_c(T)$ normalized by L^3/σ_A^3 (averaged over 1000 trajectories) during the cooling (squares) and heating (circles) protocols at rates $R_c \approx 0.5R_c^*$ and $R_h \approx 0.5R_h^*$ for LJ mixtures with diameter ratios $\alpha = 1.0, 0.97, \text{ and } 0.95$. For all systems, the maximum number of crystal clusters is larger for the heating protocol compared to that for the cooling protocol and N_c^{\max} decreases with increasing glass-forming ability (decreasing α).

asymmetry ratio $R_h^*/R_c^* > 1$, and that the ratio grows with increasing GFA (increasing diameter ratio) and decreasing R_p . We find that CNT can qualitatively describe the dependence of the asymmetry ratio on the GFA, as measured by the critical cooling rate R_c^* , for both our MD simulations and recent experiments on BMGs, as well as on the preparation cooling rate R_p for the MD simulations.

A. Intrinsic asymmetry ratio

The critical heating and cooling rates can be obtained by fitting the probability for crystallization $P(R_{h,c})$ as a function of R_h or R_c to the sigmoidal form in Eq. (6). We first investigate the minimum value for the asymmetry ratio $R_h^*(\infty)/R_c^*$, which is obtained by taking the $R_p \rightarrow \infty$ limit. [The asymmetry ratio $R_h^*(R_p)/R_c^*$ for finite preparation rates R_p will be considered in Sec. III C.] In Fig. 4, we plot $R_h^*(\infty)/R_c^*$ versus R_c^* (for diameter ratios $\alpha = 1.0, 0.97, 0.96, 0.95, \text{ and } 0.93$). We find that $R_h^*(\infty) > R_c^*$ for all systems studied, which is consistent with classical nucleation theory (CNT). As shown in Fig. 1, more crystal nuclei form during the heating protocol than during the cooling protocol. In addition, CNT predicts that the growth rates for crystal nuclei are larger during heating compared to cooling. In Sec. III B, we will show that both factors contribute to an increased probability for crystallization during heating.

In Fig. 4, we also show that the asymmetry ratio $R_h^*(\infty)/R_c^*$ increases as the critical cooling rate R_c^* decreases, or equivalently as the glass-forming ability increases. In the MD simulations, we were able to show a correlation between the asymmetry ratio and the critical cooling rate over roughly an order of magnitude in R_c^* . In Sec. III B, we introduce a model that describes qualitatively this dependence of the asymmetry ratio on R_c^* .

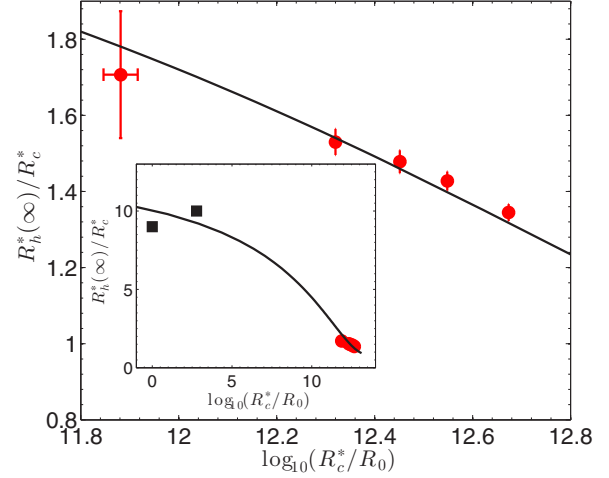


FIG. 4. (Color online) Intrinsic asymmetry ratio $R_h^*(\infty)/R_c^*$ versus the critical cooling rate R_c^* (for diameter ratios $\alpha = 1.0, 0.97, 0.96, 0.95, \text{ and } 0.93$) normalized by $R_0 = 1 \text{ K/s}$ on a logarithmic scale. The inset shows the intrinsic asymmetry ratio versus $\log_{10} R_c^*/R_0$ on an expanded scale. The filled circles indicate data from the MD simulations and filled squares indicate data from experiments on Zr- and Au-based BMGs [15,16]. The prediction [Eq. (12)] from classical nucleation theory (solid line) with $A' = (8\pi AD_0^4)/3a^3 = 0.5$ [in units of $\epsilon^2/(m^2\sigma_A^4)$], $\Sigma = 0.26$, and $Q_{\text{eff}} = 2.6$ interpolates between the MD simulation data at high R_c^* and experimental data from BMGs at low R_c^* .

B. Classical nucleation theory prediction for the asymmetry ratio

In classical nucleation theory (CNT), the formation of crystals is a nucleation and growth process: fluctuations in the size of crystal nuclei that allow them to reach the critical radius r^* , and then growth of postcritical nuclei with $r > r^*$. Several recent studies [37–39] have explored a two-step mechanism for nucleation in supercooled liquids. In the current study, we measure the asymmetry in the critical cooling and heating rates, which is not sensitive to the nucleation mechanism.

To form a critical nucleus, the system must overcome a nucleation free-energy barrier:

$$\Delta G^* = \frac{16\pi}{3} \frac{\Sigma^3}{\Delta G^2}, \quad (8)$$

where ΔG is the bulk Gibbs free-energy difference per volume (in units of ϵ/σ_A^3) and Σ is the surface tension between the solid and liquid phases (in units of ϵ/σ_A^2). We assume that $\Delta G = c(T_m - T)$ [40], where T_m is melting temperature, $T_m - T$ is the degree of undercooling, and $c \sim L_v/T_m$ is a dimensionless parameter that characterizes the thermodynamic drive to crystallize and will be used to tune the GFA of the system (where L_v is the latent heat of fusion). Within CNT, the rate of formation of critical nuclei (i.e., the nucleation rate) is given by

$$I = AD_0 \exp\left(-\frac{Q_{\text{eff}}}{T}\right) \exp\left(-\frac{\Delta G^*}{T}\right), \quad (9)$$

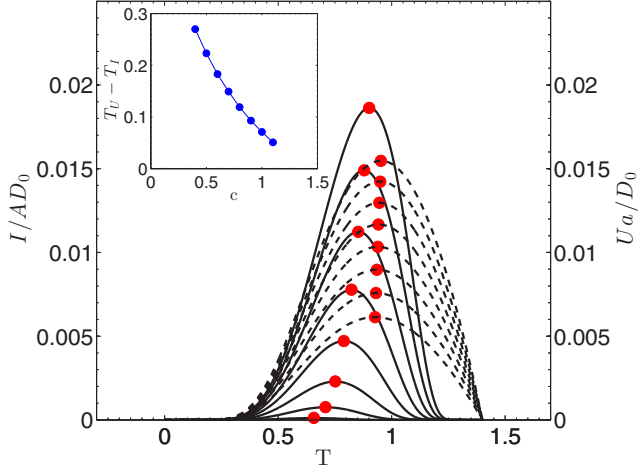


FIG. 5. (Color online) The nucleation I/AD_0 (solid lines; left axis) and growth Ua/D_0 (dashed lines; right axis) rates as a function of temperature T for increasing values of the glass-forming ability (GFA) $c = 1.2, 1.1, 1.0, 0.9, 0.8, 0.7, 0.6$, and 0.5 (from top to bottom) that span the range of diameter ratios from $\alpha = 1.0$ to 0.93 . The filled circles indicate the maximum rates (I^* and U^*) for each GFA. As the GFA increases, I^* and U^* decrease and the difference $T_U - T_I$ between the temperatures at which the maxima in $U(T)$ and $I(T)$ occur increases (inset).

where A is an $O(1)$ constant with units σ_A^{-5} , D_0 is the atomic diffusivity with units $\sigma_A \sqrt{\epsilon/m}$, and Q_{eff} is an effective activation energy for the diffusivity with units ϵ . After the nucleation free-energy barrier ΔG^* has been overcome and crystal nuclei reach $r \geq r^*$, the growth rate of crystal nuclei is given by

$$U = \frac{D_0}{a} \exp\left(-\frac{Q_{\text{eff}}}{T}\right) \left[1 - \exp\left(-\frac{\Delta GV}{T}\right)\right], \quad (10)$$

where a the characteristic interatomic spacing.

In Fig. 5, we plot the nucleation I/AD_0 and growth rates Ua/D_0 with $Q_{\text{eff}} = 2.6$ and $T_m \approx 1.40$ from MD simulations of binary LJ systems [41], $\Sigma = 0.26$, which is typical for BMGs [15], while varying the GFA parameter from $c = 1.2$ to 0.5 (corresponding to diameter ratios from $\alpha = 1.0$ to 0.93). Both $I(T)$ and $U(T)$ are peaked with maxima I^* and U^* at temperatures T_I and T_U . In Fig. 5, we show that as the GFA increases, I^* and U^* , as well as T_I and T_U decrease. However, T_I decreases faster than T_U , so that the separation between the peaks, $T_U - T_I$, increases with GFA.

To determine the critical heating and cooling rates, R_h^* and R_c^* , we must calculate the fraction of the samples N_X that crystallize and the probability for crystallizing $P(R_{h,c}) = N_X/N_{\text{tot}}$, where N_{tot} is the total number of samples, upon heating and cooling. Within classical nucleation theory, the probability to crystallize upon cooling from T_i to T_f is given by [42]

$$P(R_c) = \frac{4\pi}{3R_c^4} \int_{T_i}^{T_f} I(T') \left[\int_{T'}^{T_f} U(T'') dT'' \right]^3 dT'. \quad (11)$$

We assume that T_i is above the liquidus temperature T_l , and T_f is below the glass transition temperature T_g , where the time required to form crystal nuclei diverges. We can rearrange Eq. (11) to solve for the critical cooling rate at which $P(R_c^*) = 0.5$:

$$\begin{aligned} (R_c^*)^4 &= \frac{8\pi}{3} \int_{T_i}^{T_f} I(T') \left[\int_{T'}^{T_f} U(T'') dT'' \right]^3 dT' \\ &= A' \int_{T_i}^{T_f} dT' \exp\left(-\frac{Q_{\text{eff}}}{T'}\right) \exp\left(-\frac{\Delta G^*}{T'}\right) \\ &\quad \times \left[\int_{T'}^{T_f} \exp\left(-\frac{Q_{\text{eff}}}{T''}\right) \left[1 - \exp\left(-\frac{\Delta GV}{T''}\right)\right] dT'' \right]^3, \end{aligned} \quad (12)$$

where $A' = (8\pi AD_0^4)/(3a^3)$ and we assumed that A , D_0 , and a are independent of temperature. A similar expression for the intrinsic critical heating rate $R_h^*(\infty)$ can be obtained by reversing the bounds of integration in Eq. (12).

In Fig. 4, we plot the intrinsic asymmetry ratio $R_h^*(\infty)/R_c^*$ predicted from Eq. (12) versus the critical cooling rate R_c^* after choosing the best value $A' = 0.5$ that interpolates between the MD simulation data at high R_c^* and experimental data from BMGs at low R_c^* . We find that CNT qualitatively captures the increase in the asymmetry ratio with increasing GFA over a wide range of critical cooling rates from 1 K/s (experiments on BMGs) to 10^{12} K/s (MD simulations of binary LJ systems). A comparison of Figs. 4 and 5 reveals that the increase in the intrinsic asymmetry ratio is caused by the separation of the peaks in the growth and nucleation rates $U(T)$ and $I(T)$ that occurs as the GFA increases. Thus, we predict an enhanced value for $T_U - T_I$ in experiments on BMGs since the critical cooling rate in experiments is orders of magnitude smaller than in the MD simulations.

The fact that $R_h^*(\infty) > R_c^*$ is also reflected in the asymmetry of the “nose” of the time-temperature-transformation (TTT) diagram. In Fig. 6, we show the probability P that the system has crystallized at a given temperature T after a waiting time t for monodisperse LJ systems. We find that $T_{\text{min}} \sim 0.5\text{--}0.6$ is the temperature at which the waiting time for crystallization is minimized and that the time to crystallize is in general longer for $T < T_{\text{min}}$ compared to $T > T_{\text{min}}$. Because crystallization on average occurs at a higher temperature during heating and a lower temperature during cooling, the asymmetry in the TTT diagram indicates that slower rates are required to crystallize during cooling than during heating, i.e., $R_c^* < R_h^*$.

C. Asymmetry ratio for finite R_p

In Sec. III B, we assumed that the initial samples (i.e., the zero-temperature glasses) for the heating protocol were prepared in the $R_p \rightarrow \infty$ limit and thus were purely amorphous. How does the asymmetry ratio $R_h^*(R_p)/R_c^*$ depend on R_p when the preparation cooling rate R_p is finite and partial crystalline order can occur in the samples? In this section, we show results for the asymmetry ratio $R_h^*(R_p)/R_c^*$ for monodisperse systems using a protocol where the samples are quenched from equilibrated liquid states to zero temperature at a finite rate R_p and then heated to temperature T_f at sxs rate R_h (see Sec. II A). Note that when $R_p/R_c^* \approx 1$, some

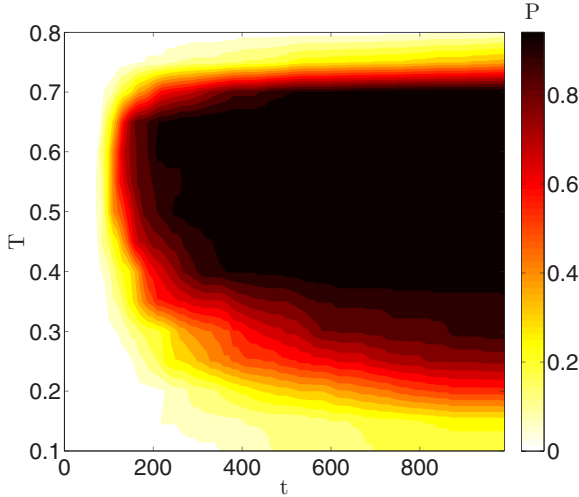


FIG. 6. (Color online) The time-temperature-transformation (TTT) diagram during cooling is visualized by plotting the probability to crystallize P (increasing from light to dark) from 96 samples as a function of temperature T and waiting time t for LJ systems with diameter ratio $\alpha = 1.0$. A sample is considered crystalline if the number of crystal-like particles satisfies $N_{cr}/N > 0.5$. The initial states are dense liquids equilibrated at $T = 2.0$. Each initial state is cooled (at rate $R_c \gg R_c^*$) to temperature $T < T_l$, where $T_l \approx 1.4$ is the liquidus temperature, and then run at fixed T for a time t .

of the samples crystallize during the cooling preparation, yet these samples are still included in the calculation of the probability $P(R_h^*(R_p))$ to crystallize. In Fig. 7, we show the results for the asymmetry ratio $R_h^*(R_p)/R_c^*$ from MD

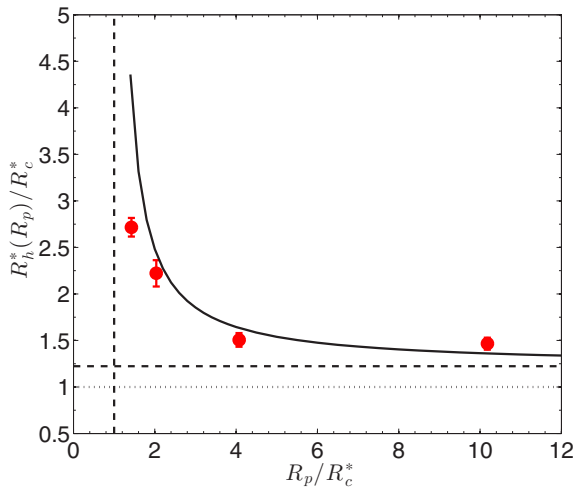


FIG. 7. (Color online) Asymmetry ratio $R_h^*(R_p)/R_c^*$ plotted versus the preparation cooling rate R_p normalized by the critical cooling rate R_c^* from MD simulations with $\alpha = 1.0$ (filled circles) and the prediction from CNT (solid line) with the same parameters used for the fit described in the legend of Fig. 4 and the GFA parameter set to $c = 1.2$. The vertical dashed line indicates $R_p = R_c^*$. The horizontal dashed lines $R_h^*(R_p)/R_c^* = 1.18$ and 1 indicate the plateau value in the $R_p \gg R_c^*$ limit and $R_h^* = R_c^*$, respectively. The gap between the horizontal dashed and dotted lines give the magnitude of the intrinsic asymmetry ratio for this particular GFA (cf. Fig. 4).

simulations. We find that $R_h^*(R_p)/R_c^*$ grows rapidly as R_p approaches R_c^* from above and reaches a plateau value of ~ 1.2 in the limit $R_p/R_c^* \gg 1$.

The critical heating rate $R_h^*(R_p)$ at finite R_p can also be calculated from CNT using an expression similar to Eq. (12) with an additional term that accounts for cooling the equilibrated liquid samples to zero temperature at a finite rate. In Fig. 7, we show that the asymmetry ratio $R_h^*(R_p)/R_c^*$ predicted using CNT agrees qualitatively with that from the MD simulations. The number of crystal nuclei that form during the quench increases with decreasing R_p , which causes $R_h^*(R_p)/R_c^*$ to diverge as $R_p \rightarrow R_c^*$. The predicted *intrinsic* contribution to the asymmetry ratio for $R_p \sim R_c^*$ is small, and $R_h^*(R_p)/R_c^*$ is dominated by the preparation protocol. In contrast, the asymmetry ratio $R_h^*(R_p)/R_c^* \approx 1.2$ is dominated by the intrinsic contribution in the $R_p \gg R_c^*$ limit. As shown in Fig. 4, the size of the intrinsic contribution to the asymmetry ratio can be tuned by varying the GFA, which controls the separation between the peaks in the nucleation $I(T)$ and growth $U(T)$ rates.

IV. CONCLUSION

We performed MD simulations of binary Lennard-Jones systems to model the crystallization process during heating and cooling protocols in metallic glasses. We focused on measurements of the ratio of the critical heating R_h^* and cooling R_c^* rates, below which crystallization occurs during the heating and cooling trajectories. We find: (1) $R_h^* > R_c^*$ for all systems studied, (2) the asymmetry ratio R_h^*/R_c^* grows with increasing glass-forming ability (GFA), and (3) the critical heating rate $R_h^*(R_p)$ has an intrinsic contribution $R_h^*(\infty)$ and protocol-dependent contribution $R_h^*(R_p) - R_h^*(\infty)$ that increases with decreasing cooling rates R_p used to prepare the initial samples at zero temperature. We show that these results are consistent with the prediction from classical nucleation theory that the maximal growth rate occurs at a higher temperature than the maximal nucleation rate and that the separation between the peaks in nucleation $I(T)$ and growth $U(T)$ rates increases with the GFA. Predictions from CNT are able to qualitatively capture the dependence of the asymmetry ratio on the GFA as measured through R_c^* for both our MD simulations and recent experiments on BMGs as well as on R_p for the MD simulations. Thus, our simulations have addressed how the thermal processing history affects crystallization, which strongly influences the thermoplastic formability of metallic glasses.

ACKNOWLEDGMENTS

The authors acknowledge primary financial support from the NSF MRSEC Grant No. DMR-1119826. We also acknowledge support from the Kavli Institute for Theoretical Physics (through NSF Grant No. PHY-1125915), where some of this work was performed. This work also benefited from the facilities and staff of the Yale University Faculty of Arts and Sciences High Performance Computing Center and the NSF (Grant No. CNS-0821132) that in part funded acquisition of the computational facilities.

- [1] J. Frenkel, *J. Chem. Phys.* **7**, 538 (1939).
- [2] R. D. Doherty, D. A. Hughes, F. J. Humphreys, J. J. Jonas, D. Juul Jensen, M. E. Kassner, W. E. King, T. R. McNelley, H. J. McQueen, and A. D. Rollett, *Mat. Sci. Eng. A-Struct.* **238**, 219 (1997).
- [3] M. Asta, C. Beckermann, A. Karma, W. Kurz, R. Napolitano, M. Plapp, G. Purdy, M. Rappaz, and R. Trivedi, *Acta Mater.* **57**, 941 (2009).
- [4] W. J. Boettinger, S. R. Coriell, A. L. Greer, A. Karma, W. Kurz, M. Rappaz, and R. Trivedi, *Acta Mater.* **48**, 43 (2000).
- [5] D. Holland-Moritz, D. M. Herlach, and K. Urban, *Phys. Rev. Lett.* **71**, 1196 (1993).
- [6] J. Schroers, D. Holland-Moritz, D. M. Herlach, and K. Urban, *Phys. Rev. B* **61**, 14500 (2000).
- [7] Y. T. Shen, T. H. Kim, A. K. Gangopadhyay, and K. F. Kelton, *Phys. Rev. Lett.* **102**, 057801 (2009).
- [8] R. Busch, *J. Mater. Sci.* **52**, 39 (2000).
- [9] K. F. Kelton, *Solid State Phys.* **45**, 75 (1991).
- [10] R. Busch, J. Schroers, and W. H. Wang, *MRS Bull.* **32**, 620 (2007).
- [11] H. Ehmeler, A. Heesemann, K. Ratzke, F. Faupel, and U. Geyer, *Phys. Rev. Lett.* **80**, 4919 (1998).
- [12] A. Masuhr, T. A. Waniuk, R. Busch, and W. L. Johnson, *Phys. Rev. Lett.* **82**, 2290 (1999).
- [13] J. H. Perepezko, *Prog. Mater. Sci.* **49**, 263 (2004).
- [14] J. H. Perepezko, R. J. Hebert, R. I. Wu, and G. Wilde, *J. Non-Cryst. Solids* **317**, 52 (2003).
- [15] J. Schroers, A. Masuhr, W. L. Johnson, and R. Busch, *Phys. Rev. B* **60**, 11855 (1999).
- [16] S. Pogatscher, P. J. Uggowitzer, and J. F. Löffler, *Appl. Phys. Lett.* **104**, 251908 (2014).
- [17] J. Schroers, *Adv. Mater.* **22**, 1566 (2010).
- [18] J. Schroers, *Phys. Today* **66**, 32 (2013).
- [19] W. L. Johnson, G. Kaltenboeck, M. D. Demetriou, J. P. Schramm, X. Liu, K. Samwer, C. P. Kim, and D. C. Hofmann, *Science* **332**, 828 (2011).
- [20] B. Pitt, G. Kumar, and J. Schroers, *J. Appl. Phys.* **110**, 043518 (2011).
- [21] Z. P. Lu and C. T. Liu, *Acta Mater.* **50**, 3501 (2002).
- [22] K. Zhang, M. Wang, S. Papanikolaou, Y. Liu, J. Schroers, M. D. Shattuck, and C. S. O'Hern, *J. Chem. Phys.* **139**, 124503 (2013).
- [23] W. Kob, *J. Phys.: Condens. Matter* **11**, R85 (1999).
- [24] G. Johnson, A. I. Mel'cuk, H. Gould, W. Klein, and R. D. Mountain, *Phys. Rev. E* **57**, 5707 (1998).
- [25] N. Nishiyama and A. Inoue, *Acta Mater.* **47**, 1487 (1999).
- [26] T. Mizuguchi and T. Odagaki, *Phys. Rev. E* **79**, 051501 (2009).
- [27] M. P. Allen and D. J. Tildesley, *Computer Simulation of Liquids* (Oxford University Press, New York, 1987).
- [28] M. A. Barroso and A. L. Ferreira, *J. Chem. Phys.* **116**, 7145 (2002).
- [29] S. Jungblut and C. Dellago, *J. Chem. Phys.* **134**, 104501 (2011).
- [30] P.-R. ten Wolde, M. J. Ruiz-Montero, and D. Frenkel, *Faraday Discuss.* **104**, 93 (1996).
- [31] P.-R. ten Wolde, M. J. Ruiz-Montero, and D. Frenkel, *J. Chem. Phys.* **104**, 9932 (1996).
- [32] R. Sedgewick and K. Wayne, *Algorithms*, 4th ed. (Addison-Wesley, New York, 2011).
- [33] E. Sanz, C. Valeriani, E. Zaccarelli, W. C. K. Poon, M. E. Cates, and P. N. Pusey, *Proc. Natl. Acad. Sci. USA* **111**, 75 (2014).
- [34] S. Auer and D. Frenkel, *J. Chem. Phys.* **120**, 3015 (2004).
- [35] L. Filion, M. Hermes, R. Ni, and M. Dijkstra, *J. Chem. Phys.* **133**, 244115 (2010).
- [36] W. Mickel, S. C. Kapfer, G. E. Schröder-Turk, and K. Mecke, *J. Chem. Phys.* **138**, 044501 (2013).
- [37] J. Russo and H. Tanaka, *Sci. Rep.* **2**, 505 (2012).
- [38] T. Schilling, H. J. Schöpe, M. Oettel, G. Opletal, and I. Snook, *Phys. Rev. Lett.* **105**, 025701 (2010).
- [39] T. Kawasaki and H. Tanaka, *Proc. Natl. Acad. Sci. USA* **107**, 14036 (2010).
- [40] D. A. Porter, K. E. Easterling, and M. Y. Sherif, *Phase Transformations in Metals and Alloys*, 3rd ed. (CRC Press, Boca Raton, 2009).
- [41] K. Meier, A. Laesecke, and S. Kabelac, *J. Chem. Phys.* **121**, 9526 (2004).
- [42] C. Suryanarayana and A. Inoue, *Bulk Metallic Glasses* (CRC Press, Boca Raton, 2011).